energies

MDPI

Article

Analysis of Onshore Synthetic Inertia and Primary Control Reserve Contributions of Alternating Current-Side Meshed Offshore Grids with Voltage-Source Converter and Diode Rectifier Unit High-Voltage Direct Current Connections

Michael Herrmann *, Merlin Alkemper and Lutz Hofmann

Institute of Electric Power Systems, Electric Power Engineering Section, Leibniz University Hannover, 30167 Hanover, Germany; alkemper@stud.uni-hannover.de (M.A.); hofmann@ifes.uni-hannover.de (L.H.)
* Correspondence: herrmann@ifes.uni-hannover.de

Abstract: The increasing use of renewable energy sources in place of conventional generation units is leading to a reduction in onshore inertia and to the development of offshore wind park grids connected by multiple high-voltage direct current (HVDC) connections to the onshore alternating current (AC) grid. For AC-side meshed offshore grids with voltage-source converter (VSC) and diode rectifier unit (DRU) HVDC connections towards onshore grids, this study focuses on the energetic feasibility of synthetic inertia (SI) and primary control reserve (PCR) contributions triggered locally at the onshore converters of both connection types. To this end, the obstacles preventing contributions for VSC HVDC connections and the mechanisms allowing contributions for DRU HVDC connections are identified first. Based on these findings, the article proposes an enhancement of the offshore HVDC converter controls that is continuously active and allows locally triggered onshore contributions at all onshore HVDC converters of both connection types without using communication and requiring only minimal system knowledge. Additional simulations confirm that, although the enhancement is continuously active, the operational performance of the offshore HVDC converter controls for normal offshore grid operation and its robustness against offshore AC-side faults are not affected.

Keywords: synthetic inertia; primary control reserve; offshore grid; HVDC; voltage-source converter; diode rectifier unit; HVDC converter control; offshore control concept

Citation: Herrmann, M.; Alkemper, M.; Hofmann, L. Analysis of Onshore Synthetic Inertia and Primary Control Reserve Contributions of Alternating Current-Side Meshed Offshore Grids with Voltage-Source Converter and Diode Rectifier Unit High-Voltage Direct Current Connections. *Energies* **2023**, *16*, 6700. https://doi.org/10.3390/en16186700

Academic Editors: Robert Schuerhuber, Ziqian Zhang and José Matas

Received: 31 July 2023
Revised: 12 September 2023
Accepted: 15 September 2023
Published: 19 September 2023

1. Introduction

1.1. Motivation

With the increasing use of renewable energy sources and the coinciding decommissioning of conventional generation units to meet the European goals for reducing greenhouse gas emissions, a fundamental change in the electrical power system is taking place [1,2]. This change involves a decrease in inertia within the onshore grid, as conventional generation units usually involve synchronous generators with rotating masses, whereas renewable generation is connected by power electronic inverters instead [3,4]. Being directly related to frequency stability, the decrease in inertia is closely monitored by the European Network of Transmission System Operators (ENTSO-E) and, amongst others, addressed in the European Union (EU)-funded projects MIGRATE (Massive Integration of Power Electronic Devices) and RE-SERVE (Renewables in a Stable Electric Grid) [3–7].

At the same time, the increasing use of renewable energy sources is reflected by ambitious development goals, e.g., for offshore wind parks (OWPs). According to the European strategy for offshore renewable energy, the EU-wide installed capacity of OWPs should reach 60 GW by 2030 and 340 GW by 2050 [8]. Recently, nine countries adjacent to the North Sea, including Germany, made a joint commitment to install 120 GW of OWP capacity by 2030 and 300 GW by 2050 in the North Sea alone [9]. To achieve such targets,

instead of the dedicated high-voltage direct current (HVDC) connections (see Figure 1a) in a symmetrical monopolar configuration used for groups of OWPs today, increasingly more complex offshore grid structures will need to be developed in the North Sea [10,11]. In the near future, offshore grid structures with offshore alternating current (AC)-side parallel operation of HVDC connections (see Figure 1b) are expected, while in the more distant future, offshore AC-side (see Figure 1c) or offshore AC-side and direct current (DC)-side meshed grid structures (see Figure 1d) with multiple international connections are expected [10–12].

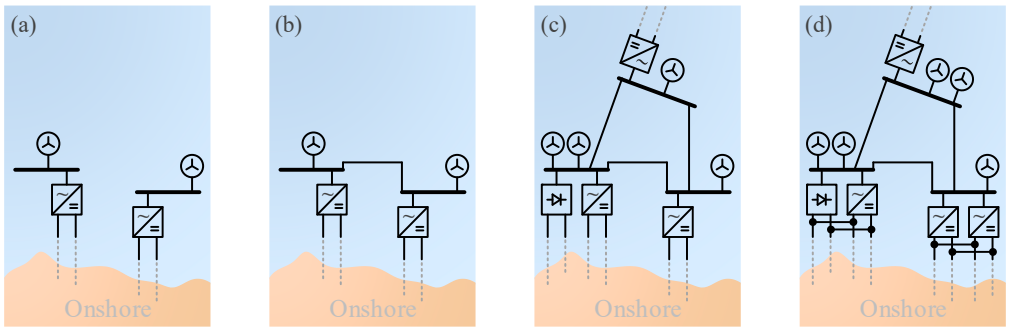

Figure 1. Expected development of the fundamental offshore grid structure of future erections: (**a**) dedicated HVDC connections; (**b**) AC-side parallel HVDC connections; (**c**) AC-side meshed HVDC connections; (**d**) AC- and DC-side meshed HVDC connections.

As illustrated in Figure 1c,d, future offshore grid structures may include HVDC connections of different technologies and bipolar configurations as well. In addition to connections using voltage-source converter (VSC) technology (see Figure 2a), which is well established for OWP connections today, connections using a passive diode rectifier unit (DRU) as an offshore converter (see Figure 2b) might also be integrated [11–13].

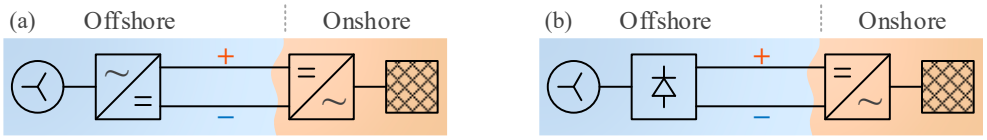

Figure 2. Use of a dedicated (**a**) VSC and (**b**) DRU HVDC connection for OWP connection.

Compared to VSC HVDC connections, DRU HVDC connections promise cost savings due to reduced space requirements on the offshore platform, less maintenance, as well as lower power losses [14,15]. According to the manufacturer, overall cost savings of up to 30% and reductions in power losses of up to 20% can be achieved [15,16]. However, these benefits come at the price of DRU converters being passive and therefore dependent on other units controlling the offshore grid voltage and frequency, such as the offshore wind turbines or other active offshore HVDC converters [14]. In addition, the AC- and DC-side voltage-dependent active power flow of DRU converters is unidirectional, and harmonic filters as well as offshore reactive power compensation are required [14,15]. Due to the need for adapted offshore wind turbine controls, no DRU HVDC connections have been used for dedicated OWP connections as of the end of 2022. More likely, therefore, is the integration of both VSC and DRU HVDC connections into more complex future offshore grid structures, as proven feasible within the EU-funded PROMOTioN (Progress on Meshed HVDC Offshore Transmission Networks) project [17] and investigated further within the government-funded German NSON II (North Seas Offshore Network II) project [18].

Against the background of future offshore grids using different HVDC technologies for international connection and the onshore decrease in inertia, the question is raised of how such offshore grids can improve the onshore grid's frequency stability by providing synthetic inertia (SI), fast frequency response (FFR), and primary control reserve (PCR)

contributions. This article evaluates the effects of onshore SI and PCR contributions on an offshore grid being AC-side meshed (see Figure 1c) and connected by VSC and DRU HVDC connections to propose enhancements to the offshore HVDC converter controls, overcoming barriers to said contributions.

1.2. Related Work and Contributions of This Article

To place this article in the context of existing research, a distinction is first made between the terms synthetic inertia, fast frequency response, and primary control reserve contribution for converter responses to grid disturbances, as there are a variety of understandings. In this article, SI refers to near-instantaneous changes in the converter's output voltage phasor due to grid disturbances, e.g., based on power measurements, and, therefore, inherent active power responses [13,19]. In contrast, FFR refers to all active power responses based on frequency (derivative) measurements, naturally delayed, to deduce corresponding changes in active power dispatch [13,19]. PCR is activated in the same way as FFR, but on a slower time scale and with the requirement to be maintained longer [20]. While SI, FFR, and PCR contributions improve the frequency nadir, only SI contributions are able to influence the gradient of frequency at the moment of disturbance [13,19]. The terms SI, FFR, and PCR are used below as defined, regardless of the terminology used in the references cited. As of the end of 2019, only the German grid code addresses an SI requirement for HVDC connections based on the network code HVDC [13,21–23]. The implementation of this requirement as SI or FFR is to be coordinated with the responsible transmission system operator [24].

For OWPs connected by a single VSC HVDC connection, FFR contributions, in particular, are studied in the literature [25–34]. The required energy is inherently taken from the DC link of the HVDC connection, thereby lowering the DC voltage. While the feasibility and the benefit during onshore grid disturbances are demonstrated in [25,26], the amount of energy that can be extracted before the lowered DC voltage restricts the operation of the HVDC converters is very limited [26]. In order to utilize additional energy from the OWP, e.g., energy retained by wind turbine (WT) curtailment or stored within the rotating masses of the WTs, additional mechanisms need to be implemented. These mechanisms can be classified according to their use of long-distance communication between the onshore HVDC converter and the offshore grid [35,36]. With long-distance communication, the required contributions detected at the onshore HVDC converter are communicated to the offshore WTs, which change their active power dispatch to provide the required contributions [27]. Such mechanisms allow for contributions to FFR and also PCR, but, given detection and communication, are not capable of SI contributions. Without long-distance communication, the offshore HVDC converter must either translate offshore DC voltage changes caused by onshore contributions into offshore grid frequency changes [28–30] or communicate such DC voltage changes to the offshore WTs via short-distance communication [31–33]. In both cases, the WT controls will need to be modified to respond accordingly to frequency changes or communication signals [28–33]. In addition, to avoid changes in WT active power dispatch at times when no contributions are required, the offshore DC voltage needs to be kept nearly constant. For this purpose, the author of [34] proposes a dynamic onshore DC voltage setpoint calculation using the HVDC active power transmission. Both mechanisms without long-distance communication allow for contributions to FFR and PCR, but also SI, e.g., by applying instantaneously reacting onshore HVDC converter controls with swing equation emulation [31,33,36]. A general overview of HVDC converter controls with swing equation emulation is given in [36]. However, in the context of OWP connections, none of the references cited in this paragraph focus on the effects of onshore HVDC converter contributions to SI on the DC link and the offshore grid supplying the energy.

For OWPs connected by multiple VSC HVDC connections, mainly FFR and PCR contributions of DC-side meshed connections are focused on in the literature, while SI contributions are not explicitly addressed [37–41]. Overall, similar findings as for single VSC HVDC connections are obtained. In [37], the mechanism presented in [25] is adapted

for use with DC-side meshed HVDC connections, further on using only the very limited energy stored in the DC link. As a result, only FFR and no PCR contributions are possible [37]. Furthermore, the mechanism requires preselection, i.e., that the contributing behavior is assigned exclusively to one of the onshore HVDC converters [37]. For the utilization of additional energy from the OWP, [38] compares mechanisms with and without long-distance communication for PCR contributions, highlighting the difficulties of avoiding communication such as unwanted droop interactions of HVDC converters. Using long-distance communication, [39] proposes a mechanism for FFR contributions, but the ineligibility of SI contributions due to measurement delays remains. In contrast, the authors of [40,41] couple offshore DC voltage and offshore grid frequency to avoid long-distance communication. By this, aside from FFR and PCR contributions, SI contributions are also feasible, although not investigated further [40,41]. In addition to the previously mentioned prerequisites for using such a mechanism for single VSC HVDC connections, it cannot easily be implemented for offshore AC-side parallel and meshed HVDC connections, as the frequency of the offshore grid cannot be defined by more than one HVDC converter without further coordination.

For OWPs connected by a single DRU HVDC connection, which naturally requires grid-forming WT controls [42–47], contributions to FFR [43,47] and PCR [42–46] are studied in the literature. In [42,43,47], mechanisms using long-distance communication are evaluated, with the delays involved again preventing contributions to SI. A mechanism based on communicating the offshore DC voltage to the WTs in order to detect ongoing contributions is proposed in [44], but neglects the need for an otherwise constant offshore DC voltage. The mechanism presented in [45] detects ongoing contributions locally in the WT controllers by offshore AC voltage deviations, but it is not clarified to what extent the mechanism interferes with normal offshore grid operation, e.g., for changes in WT generation, when no onshore contributions are required. Finally, [46] compares mechanisms with and without long-distance communication for PCR contributions and demonstrates the feasibility of avoiding such communication. However, more complex offshore grid structures using DRU HVDC connections or the offshore effects of onshore SI contributions are not found in the literature. The same applies to offshore grid structures using both VSC and DRU HVDC connections.

Against this background, the article at hand contributes a first study on onshore SI and PCR contributions of an AC-side meshed offshore grid including both VSC and DRU HVDC connections. For a given grid model and HVDC converter controls, the first objective of the study is to point out the differences between VSC and DRU HVDC connections in terms of contribution feasibility, as the required energy has to be provided by the offshore grid. These differences have not been addressed in the literature so far. The second objective of the study is to propose an enhancement to the offshore HVDC converter controls to allow offshore energy provision and subsequently SI and PCR contributions at all onshore HVDC converters of such grid structures, avoiding a converter preselection for contributions and naturally also including the feasibility of FFR contributions. As locally triggered SI contributions are targeted, the enhancement does not make use of communication for the contribution. To keep the enhancement to a minimum, it only applies to the offshore HVDC converter controls and not the WT controls. Furthermore, it is ensured that the enhancement does not negatively affect the behavior of the HVDC converter controls during normal operation and faults, when no contributions are required.

The article is structured as follows. A grid model overview and a description of the HVDC converter controls are provided in Section 2. The simplified modeling of onshore SI and PCR contributions in the context of the study objectives is presented in Section 3. Section 4 examines the feasibility of the above-mentioned onshore contributions for both VSC and DRU HVDC connections and highlights the inherent sources of the required energy. In Section 5, the offshore HVDC converter control enhancement is proposed, and its characteristics are demonstrated and discussed in Section 6. The impacts of the enhancement on normal operation and fault behavior are evaluated in Section 7. Section 8

concludes the study by summarizing the main findings and highlighting ideas for further research.

2. Modeling

The simulations were performed as electromagnetic transient (EMT) simulations in DIgSILENT PowerFactory 2019 SP4 (Gomaringen, Germany) and automated using Python 3.5 (Beaverton, OR, USA). Due to the modeling depth, only an overview of the grid model originating from the German NSON II project is given, while the study-relevant HVDC converter controls are described in detail. The complete grid model dataset is available online [48]. The descriptions are based on the corresponding project reports [49,50], which are, however, only available in German.

2.1. Grid Model

Figure 3 shows the layout of the symmetrical three-phase grid model. The grid model contains three offshore main nodes (A, B, C) mutually interconnected by multiple cable systems, with six OWPs and five VSC HVDC connections leading to separate onshore grid representations, which are not connected to each other otherwise. The total rated HVDC transmission power and the total rated OWP power are 4500 MW each. The assumed OWP topology and the grid model parameters used are based on real OWP connections in the German North Sea [49]. For the WT and VSC HVDC converters, average value models that behave like a voltage source behind an impedance are used, neglecting the harmonics introduced by switching operations.

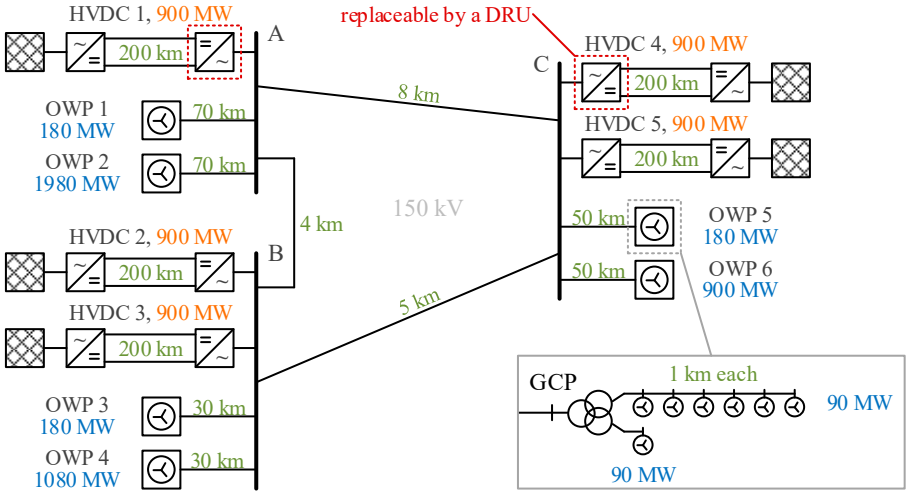

Figure 3. Layout of the offshore AC-side meshed grid model with the three main nodes A, B and C and with indication of the cable connection lengths (green), rated HVDC transmission power (orange), and rated OWP power (blue) [50].

The OWPs in Figure 3 use type 4 WTs with a rated voltage of 66 kV AC and a rated power of 15 MW each. The WTs are modeled up to their DC-side capacity including the DC infeed and the DC chopper. As WT controls, the direct voltage control of [51] with a phase-locked loop (PLL) for synchronization with the offshore grid is used. The OWPs with a rated power of 180 MW (OWPs 1, 3, 5) each consist of one WT string set up in detail and one aggregated WT string of 90 MW (see Figure 3). For OWPs with higher rated power (OWPs 2, 4, 6), both WT strings are modeled as aggregated to reduce the calculation effort. Each OWP is equipped with an OWP controller according to the German offshore grid connection rules, following a $Q(V)$ slope at the corresponding grid connection point (GCP) [52].

The VSC HVDC connections in Figure 3 are assumed to be symmetrical monopoles with modular multi-level converters (MMC) and transformers at both ends and a DC

chopper on the onshore side. The key parameters of the offshore and onshore HVDC converters and their submodules (SM) are given in Table 1, while the key parameters of the DC cables are given in Table 2.

Table 1. Key parameters of the offshore and onshore VSC HVDC converters [49].

Parameter	Offshore HVDC Converter	Onshore HVDC Converter
S_r	917 MVA	971.2 MVA
P_r, Q_r	900 MW, ±127 Mvar	900 MW, +365/−293 Mvar
V_{rAC}, V_{rDC}	363 kV AC, ±320 kV DC	380 kV AC, ±320 kV DC
L_{arm}, R_{arm}	55 mH, 5.5 mΩ	55 mH, 5.5 mΩ
N_{SM}, C_{SM}	230 (per arm), 11 mF	235 (per arm), 11 mF

Table 2. Key parameters of the DC cables [49].

Parameter	R' (20 °C)	L'	G'	C'
Value	12.9 mΩ/km	157 nH/km	0 µS/km	226 nF/km

As indicated by the dashed red squares in Figure 3, the offshore converters (including their transformers) of the VSC HVDC connections 1 and/or 4 can be replaced by a passive DRU converter (see Figure 4). This turns the selected VSC HVDC connections into DRU HVDC connections and, given the choice, yields four variants of the grid model.

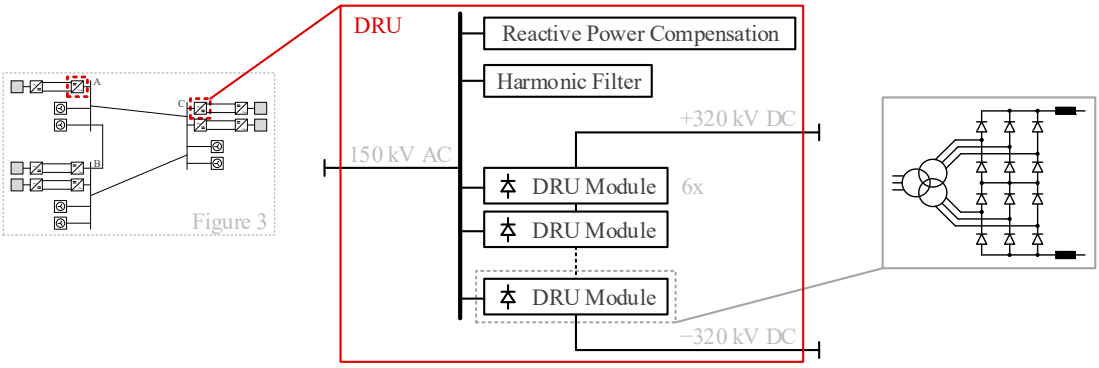

Figure 4. Layout of an offshore DRU HVDC converter including reactive power compensation and harmonic filters in the offshore grid model in Figure 3 [14–16,49,50].

2.2. Offshore HVDC Converter Controls

As DRU converters are passive, only the offshore converters of the VSC HVDC connections require controls. The description of these controls exemplarily assumes five VSC HVDC connections, but the functionality of the controls is independent of the number of VSC HVDC connections and therefore offshore VSC HVDC converters.

The offshore converter control structure (see Figure 5) is communication-based and consists of a common voltage control and one subordinate local current control for each offshore VSC HVDC converter. All control signals use per-unit (p.u.) values based on the converter rating.

In the offshore grid, the voltage phasor at node A (see Figure 3) is measured in the αβ-frame and then transformed into a dq-frame that is constantly rotating at the nominal frequency of 50 Hz. This dq-frame will be referred to as the "global dq-frame". The aim of the voltage control is to align the measured voltage phasor with a reference voltage phasor on the d-axis of the global dq-frame, thus taking over voltage, frequency, and angle control at node A. For this purpose, the voltage control requires the d- and q-axis current component contributions defined by the reference values (marked with asterisks) i^*_{dn} and i^*_{qn} to be provided, which are interpreted by the individual current controls as

active and reactive current components relative to the inner voltage source phasor of the corresponding nth converter. As a result, the offshore converters will collectively act as an active and reactive power slack within the offshore grid. The required continuous communication consists of the transmission of i^*_{dn} and i^*_{qn} from the voltage to the current controls, while the orientation of the global dq-frame can be derived from radio clock signals instead [53].

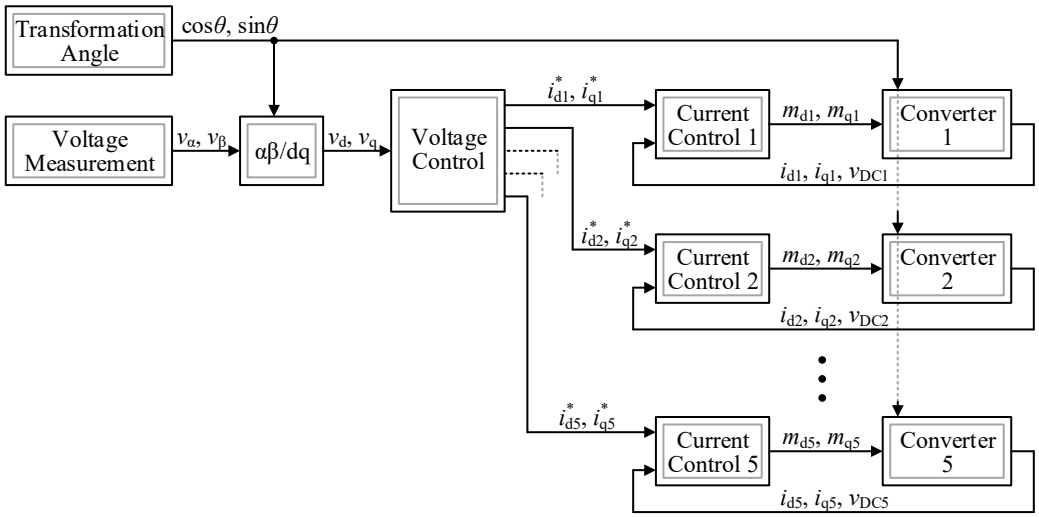

Figure 5. Structure of the offshore HVDC converter controls [50].

The block diagram of the voltage control is shown in Figure 6, with the parameters given in Table 3. The state variables of the PI controllers are initialized with the mean value of the corresponding outgoing current components so that the sum of the dynamically initialized distribution factors $K_{n\mathrm{P}}$ and $K_{n\mathrm{Q}}$ is five each. First-order low-pass filters (LPF) are used to model voltage measurement and signal processing delays. The value of 1.12 p.u. corresponds to the maximum continuous current allowed by the converters.

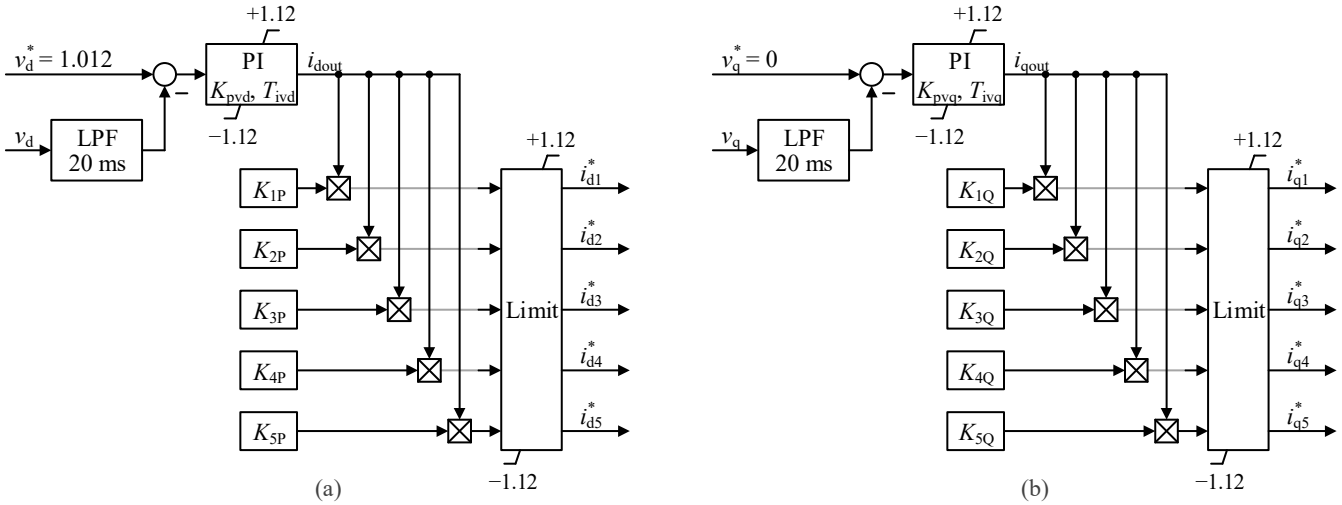

Figure 6. Block diagram of the voltage control in Figure 5: (**a**) d-axis component control path; (**b**) q-axis component control path [50].

Table 3. Parameters of the voltage control in Figure 6 [50].

Parameter	Value	Parameter	Value
K_{pvd}	0.2	K_{pvq}	30
T_{ivd}	0.15 s	T_{ivq}	0.15 s

Figure 7 shows the block diagram of the current controls of each converter from Figure 5 with the count variable n omitted from the signal names. All current controllers are equipped with the same parameters listed in Table 4. The novelty of the current control is that, in addition to the global dq-frame, a local dq-frame is used. The angle θ_t of the local dq-frame within the global dq-frame is not derived by a PLL tracking the angle of a measured voltage phasor, but is derived directly from the modulation index phasor outputted by the current control [54]. This way, the d-axis of the local dq-frame is aligned with the inner voltage source phasor of the converter in a steady state. Applying the rotational transformation between the global and local dq-frame to all input and output phasors, except the current reference phasor, makes using the local dq-frame invisible from outside the current control, but allows for interpreting i^*_d and i^*_q as active and reactive current components.

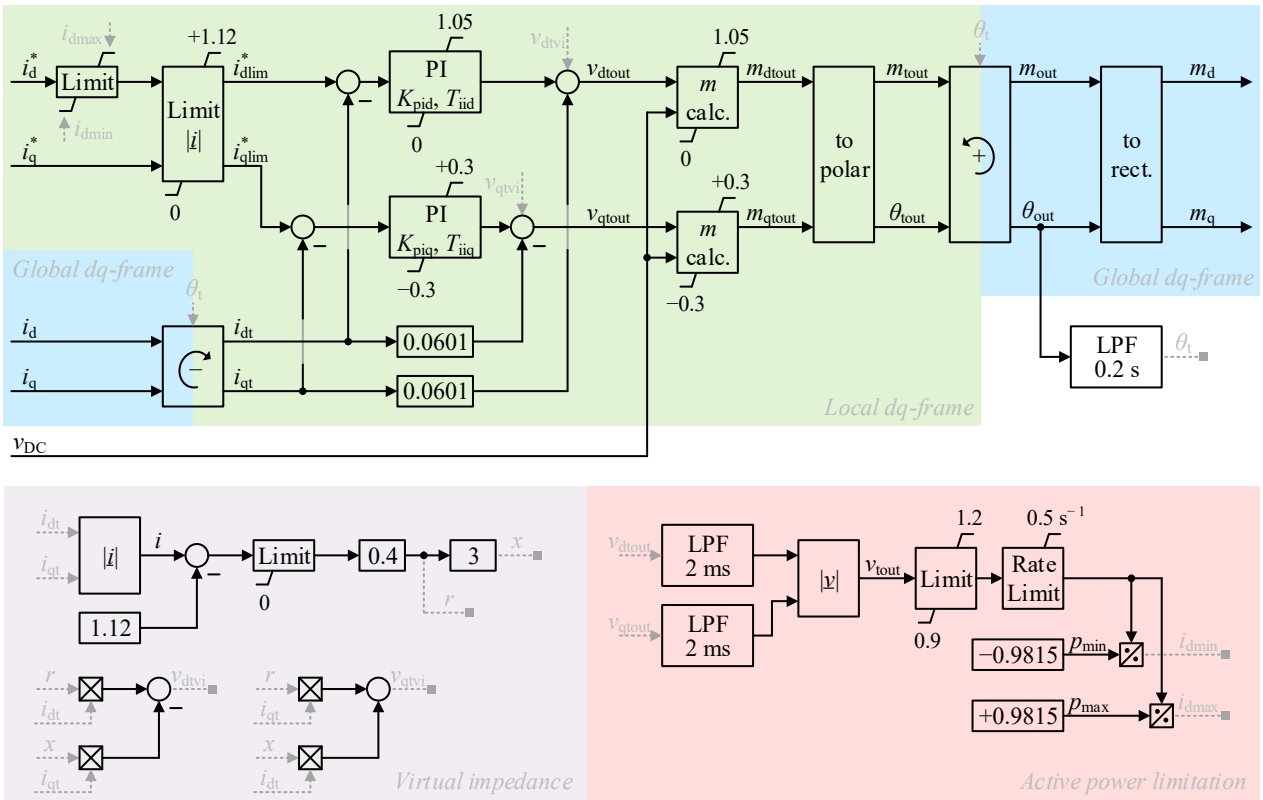

Figure 7. Block diagram of the current controls of each converter in Figure 5 with the distinct components highlighted in different colours [50].

Table 4. Parameters of the current controls in Figure 7 [50].

Parameter	Value	Parameter	Value
K_{pid}	0.8	K_{piq}	0.8
T_{iid}	10 ms	T_{iiq}	10 ms

The limits applied to the calculated d- and q-axis modulation index components (1.05 p.u. and 0.3 p.u., respectively) allow a maximum modulation index phasor magnitude

of ≈1.10 p.u. This value grants a slight overmodulation, but is below the value of ≈1.15 p.u. that can be achieved with third harmonic injection [55]. However, only the fundamental frequency is considered in the converter model.

To limit the converter currents in the event of AC-side faults, the current controls in Figure 7 apply the threshold virtual impedance from [56] directly to the output voltage phasor components. Furthermore, the reference value for the d-axis current component is limited to a voltage-dependent range corresponding to an active power transmission between −900 MW and +900 MW (−0.9815 p.u. and +0.9815 p.u.) [50].

2.3. Onshore HVDC Converter Controls

For both VSC and DRU HVDC connections, each onshore converter independently applies the control structure shown in Figure 8, so a counting variable in the signal names is not necessary. All signals use p.u. values based on the converter rating.

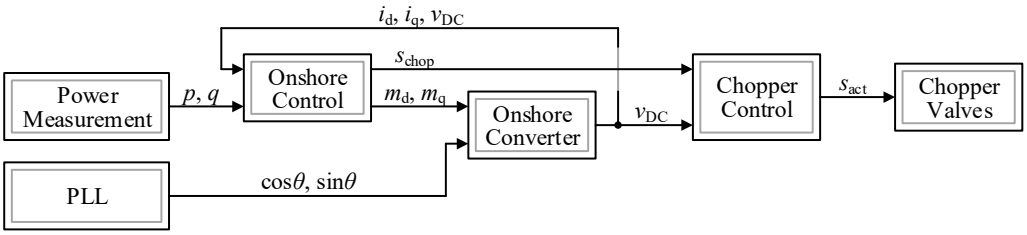

Figure 8. Structure of the onshore HVDC converter controls [50].

Active and reactive power are measured at the AC-side terminals of the converter. For the PLL, the standard PowerFactory model [57] is used. The HVDC chopper valves are activated when the DC voltage exceeds 1.2 p.u. and deactivated when it falls below 1.1 p.u. again. The signal s_{chop} allows chopper valve activation during the Emergency Power Control 1 (EPC1) system automatic required by the German grid code [23].

The block diagram of the onshore converter control in Figure 9 is equipped with the parameters in Table 5. The control variables are the AC-side reactive power exchange q and the DC-side voltage v_{DC} of the converter. By standard, s_{select} is zero, so the upper inputs of the selection blocks are active. During EPC1, s_{select} is set to one, which activates the lower inputs of the selection blocks, freezes the upper left PI controller, and passes the output signal of the EPC1 block instead. As only the existing selection blocks and not the EPC1 system automatic will be used in this study, no description of the EPC1 block is given.

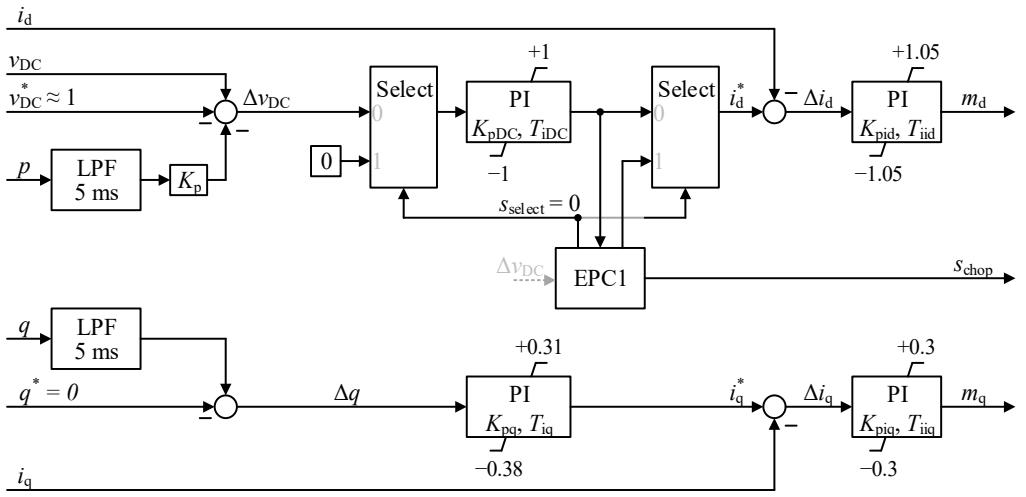

Figure 9. Block diagram of the onshore converter controls in Figure 8 [50].

Table 5. Parameters of the onshore converter controls in Figure 9 [50].

Parameter	Value	Parameter	Value
K_{pDC}	10	K_{pq}	5
T_{iDC}	5 ms	T_{iq}	100 s
K_{pid}	2	K_{piq}	2
T_{iid}	2 ms	T_{iiq}	2 ms
K_p	0.01 [1]		

[1] Valid for VSC HVDC connections only; for DRU HVDC connections, K_p is set to 0.

3. Simplified Modeling of Onshore SI and PCR Contributions

During inherent SI contributions, the active power response of the onshore HVDC converter is deliberately not shaped by the objective of DC voltage control. As this study focuses on the energetic feasibility of contributions rather than on their onshore impacts, and thus only simplified onshore grid representations are included, the detailed modeling of the mechanisms of SI and PCR contributions is not necessary. Instead, a simplified modeling approach in the form of a manually triggered active power schedule is adopted, temporarily replacing the objective of DC voltage control and resembling the characteristic challenges of both SI and PCR contributions. For this purpose, the DC voltage control path of all onshore HVDC converters is extended, as shown in Figure 10. By standard, the value of the added parameter s_{id} is zero, leaving the controls unaffected. If a value other than zero is assigned to s_{id} during simulation, the left selection block will immediately freeze the subsequent PI controller. At the same time, the value of s_{did}, generated out of s_{id} by passing an LPF, is added to the active current component reference, resulting in an active power response of the converter until s_{id} is reset to zero and DC voltage control continues.

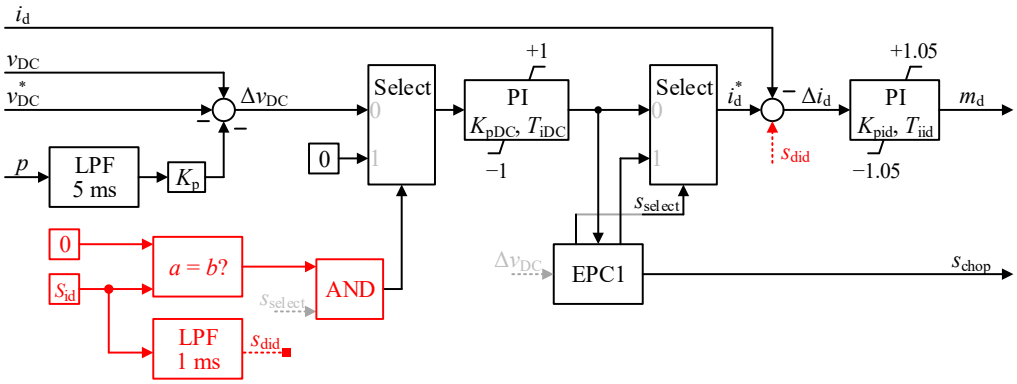

Figure 10. Block diagram of the DC voltage path of the onshore converter controls extended by the simplified modeling of onshore SI and PCR contributions (red).

In this study, the active power schedule is defined as assigning the exemplary value of +0.106 to s_{id} and resetting the value to zero 2.5 s later. The resulting AC-side active power response of an onshore converter with an assumed initial dispatch of 640 MW, with the offshore converter represented as an ideal DC voltage source, is shown in Figure 11.

The rise time (10% to 90%) of the active power response in Figure 11 of only 1.5 ms resembles the energetic challenge of inherent SI contributions. On the other hand, the amount of 100 MW and the duration of 2.5 s resemble the energetic challenge of PCR contributions. A duration of 2.5 s is manageable with the EMT models used and at the same time sufficient to determine whether a steady state is reached, and therefore, contributions of longer duration are also feasible. Consequently, the defined active power schedule can be used to determine the feasibility of both SI and PCR contributions.

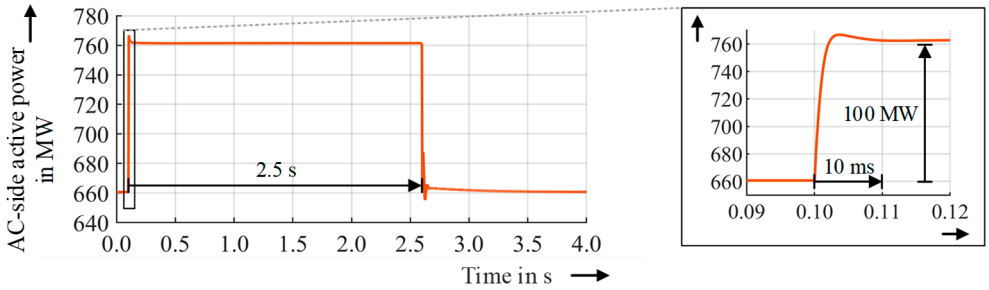

Figure 11. Active power response of an onshore HVDC converter for the defined active power schedule used to model SI and PCR contributions.

4. Feasibility and Effects of Onshore SI and PCR Contributions

For the OWPs and the HVDC connections of the grid model (see Figure 3), the initial active power operating points are assumed, as shown in Table 6. Table 6 also lists the designations of the four grid model variants (differing regarding the presence of DRU HVDC connections) that are used throughout this paper. Each result depiction will refer back to the specific grid model variant used. When a VSC HVDC connection is replaced by a DRU HVDC connection, the corresponding onshore DC voltage setpoint v^*_{DC} is chosen in a way to maintain the active power transmission of the HVDC connection. The grid model dataset uses Python scripts for setting up the four grid model variants [48].

Table 6. Grid model variant designations and initial OWP and HVDC operating points [50].

Grid Model Variant	DRU HVDC Connections	OWP	Generation [1]	HVDC	Transmission [2]
Variant 1	none	OWP 1	180 MW	HVDC 1	−682 MW
Variant 2	HVDC 1	OWP 2	1440 MW	HVDC 2	−800 MW
Variant 3	HVDC 4	OWP 3	180 MW	HVDC 3	−800 MW
Variant 4	HVDC 1, 4	OWP 4	720 MW	HVDC 4	−400 MW
		OWP 5	180 MW	HVDC 5	−300 MW
		OWP 6	360 MW		

[1] Initial total dispatch at the AC sides of all associated WT converters. [2] Initial dispatch at the AC-side terminals of the offshore HVDC converter (active sign convention).

The initial voltage at node A in Figure 3 is chosen to be 151.8 kV (1.012 p.u.). A fixed amount of the required reactive power is provided by the WTs, with the remainder provided by the offshore converters of the VSC HVDC connections in proportion to their active power dispatch. The active power schedule is only triggered at one HVDC connection at a time. Throughout this paper, the curves corresponding to VSC HVDC connections are shown as solid lines and the curves corresponding to DRU HVDC connections are shown as dotted lines.

In order to determine the contribution feasibility for AC-side meshed VSC HVDC connections, the active power schedule is triggered at HVDC 5 in grid model variant 1. As can be seen from the active power curve of the corresponding onshore converter in Figure 12a, the contribution is only feasible for a very short time. The required energy is taken from the DC link, lowering the DC voltage (see Figure 13). As the modulation index limit is reached first in the onshore converter controls, the offshore converter maintains the voltage decoupling of AC- and DC-side and therefore its active power dispatch (see Figure 12b). Consequently, the active power dispatch of the onshore converter oscillates back to its initial value, preventing any further contribution. After the active power schedule, the required restoration of the DC voltage results in a transient active power spike in the opposite direction, nullifying the total energy of the contribution.

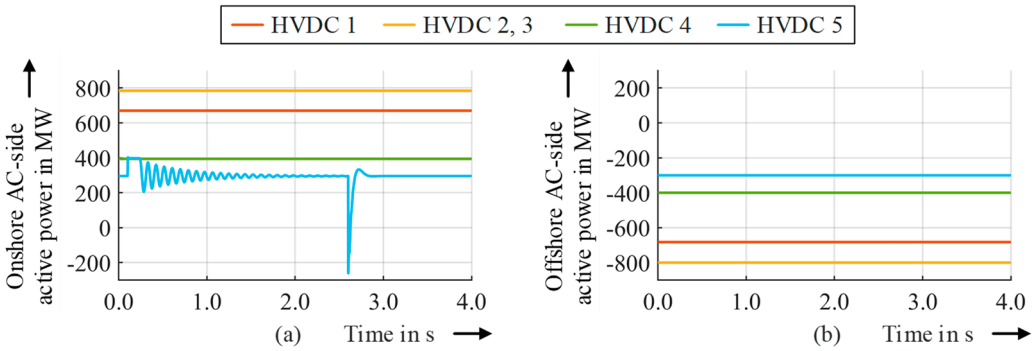

Figure 12. AC-side active power curves of the (**a**) onshore and (**b**) offshore HVDC converters for the active power schedule triggered at HVDC 5 (VSC HVDC connection) in grid model variant 1.

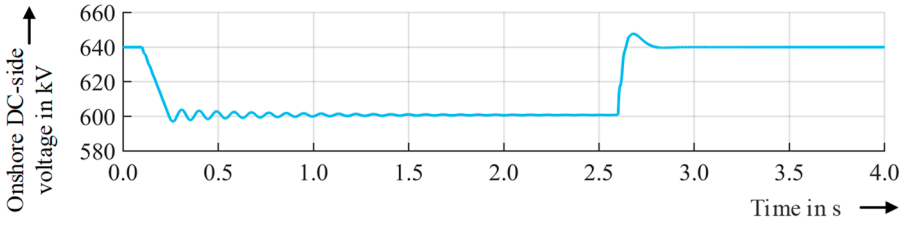

Figure 13. DC-side voltage curve at the onshore converter of HVDC 5 for the active power schedule triggered at HVDC 5 (VSC HVDC connection) in grid model variant 1.

Due to the retention of the offshore converter's active power dispatch, triggering the active power schedule at other VSC HVDC connections and in other grid model variants gives similar results. However, at some VSC HVDC connections, the active power oscillations are persistent throughout the schedule. If the modulation index limit was first reached in the offshore converter controls, this could influence the active power dispatch of the offshore converter as required. Nevertheless, as this leads to the wind-up of the offshore current control and the limit first reached depends on the off- and onshore AC voltages, the reliability of such a mechanism is questionable. Thus, without further modification, only the energy stored in the DC link is available for SI and PCR contributions of VSC HVDC connections, which is not sufficient, especially for PCR contributions.

To determine the contribution feasibility for DRU HVDC connections by analogy, the active power schedule is triggered at HVDC 1 in grid model variant 2. As can be seen from the active power curves in Figure 14a, this time the contribution is feasible for the entire duration of 2.5 s. As for VSC HVDC connections, the DC voltage is lowered at the start of the contribution (see Figure 15). However, for DRU HVDC connections, this results in a subsequent increase in the active power flow of the offshore DRU converter until a new equilibrium point is reached, drawing additional energy from the offshore grid.

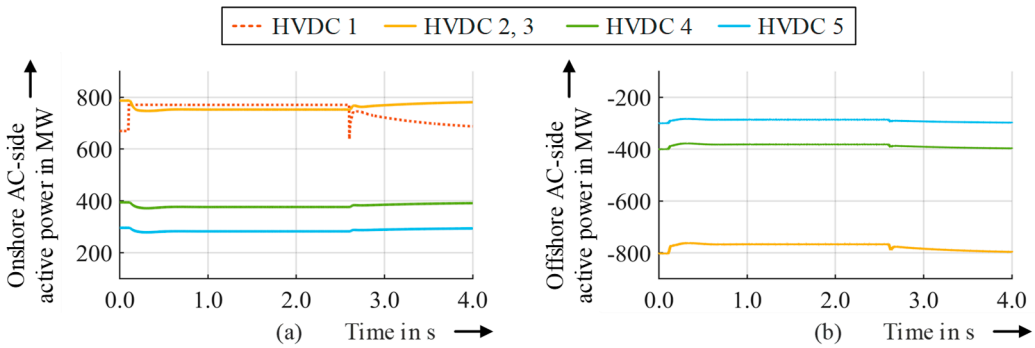

Figure 14. AC-side active power curves of (**a**) all onshore and (**b**) the offshore VSC HVDC converters for the active power schedule triggered at HVDC 1 (DRU HVDC connection) in grid model variant 2.

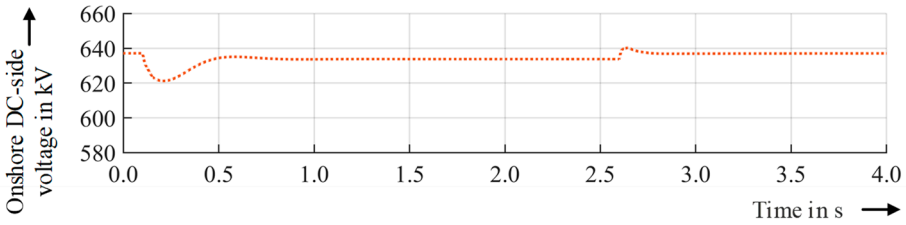

Figure 15. DC-side voltage curve at the onshore converter of HVDC 1 for the active power schedule triggered at HVDC 1 (DRU HVDC connection) in grid model variant 2.

As the offshore WTs do not inherently change their dispatch, the active power balance of the offshore grid is instead met by the offshore converters of the VSC HVDC connections, which collectively act as a slack according to the distribution factors in voltage control (see Figure 14b). Finally, the energy for the contribution is provided by the onshore grid access points of these HVDC connections (see Figure 14a). After the contribution ends, the initial operating points are restored.

For SI and PCR contributions, when more than one DRU HVDC connection is involved, it should be noted that only the onshore grid access points of the VSC HVDC connections provide the energy for the contribution, as only these connections act as a slack for the offshore grid (see curves for grid model variant 4 in Figure 16). The onshore active power and DC voltage of the DRU HVDC connection not providing the contribution are only transiently affected, especially at the start and the end of the contribution.

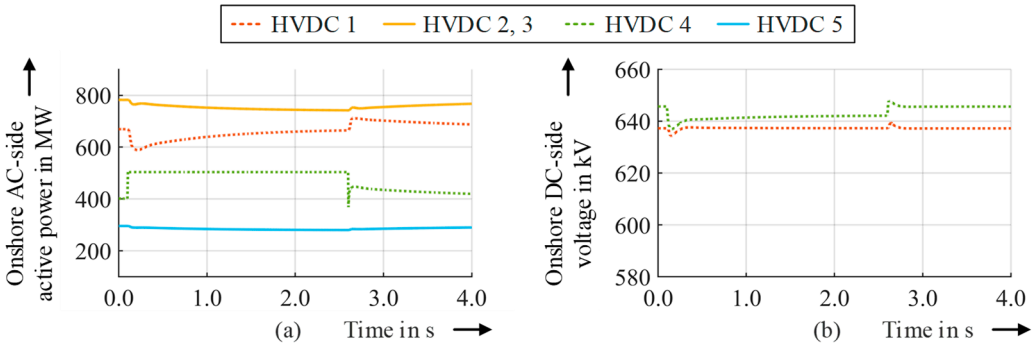

Figure 16. Onshore (**a**) AC-side active power curves of the HVDC connections and (**b**) DC-side voltage curves of the DRU HVDC connections for the active power schedule triggered at HVDC 4 (DRU HVDC connection) in grid model variant 4.

In conclusion, onshore SI and PCR contributions are by standard only feasible for DRU HVDC connections, but not for VSC HVDC connections. The feasibility is solely due to the DC voltage dependency of the active power flow of the passive DRU converter and does not require any communication.

5. Enhancement of the Offshore HVDC Converter Controls

In order to make SI and PCR contributions also feasible for VSC HVDC connections without introducing communication during contributions, each local offshore current control can be enhanced by a DC voltage dependency of the offshore active power flow similar to the DRU converter behavior. The enhancement proposed in this article is derived from the simplified steady-state equivalent circuit of the DC link, as shown in Figure 17, neglecting the inductances and branch elements, as follows.

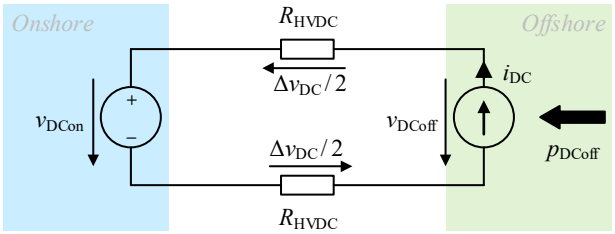

Figure 17. Simplified steady-state circuit of the DC link of a VSC HVDC connection with indication of the onshore (blue) and offshore (green) side.

In Figure 17, the direct current can be expressed as

$$i_{DC} = \frac{\Delta v_{DC}}{2 \cdot R_{HVDC}}. \tag{1}$$

Furthermore, the offshore active power can be calculated as

$$p_{DCoff} = -i_{DC} \cdot (v_{DCon} + \Delta v_{DC}). \tag{2}$$

The insertion of Equation (1) in Equation (2) yields the expression

$$p_{DCoff} = -\frac{1}{2 \cdot R_{HVDC}} \cdot \left(v_{DCon} \cdot \Delta v_{DC} + \Delta v_{DC}^2\right). \tag{3}$$

Since $\Delta v_{DC} << v_{DCon}$, the square part is neglected and the equation is rewritten as

$$\Delta v_{DC} \approx -\frac{2 \cdot R_{HVDC} \cdot p_{DCoff}}{v_{DCon}} \text{ and } v_{DCoff} = v_{DCon} + \Delta v_{DC}. \tag{4}$$

Given the DC link resistance R_{HVDC} and the onshore DC voltage v_{DCon}, Equation (4) can be used to estimate v_{DCoff} from the offshore active power p_{DCoff}. Typically, the difference between the estimated and measured offshore DC voltage is very small, while a significant difference is an indicator that an onshore contribution under the omission of the DC voltage control is occurring. The proposed control enhancement, shown in red in Figure 18, implements the relationship of Equation (4) to determine the voltage difference Δv_{DC} and multiplies this voltage difference with the gain K_{pDC} to continuously adjust the active current component reference i^*_d locally within each current control (see Figure 7).

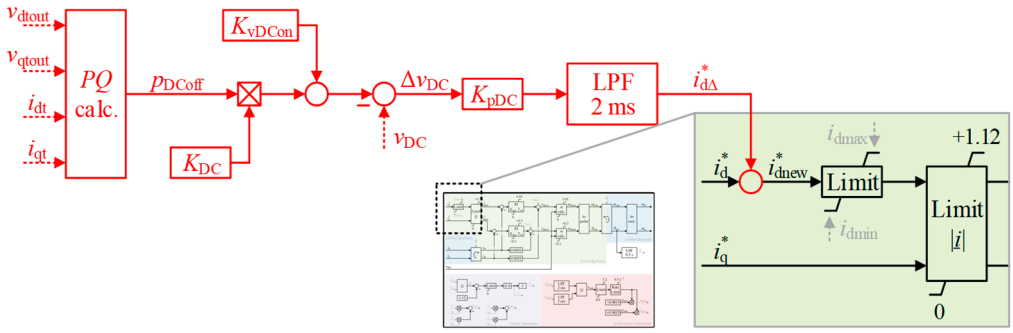

Figure 18. Block diagram of the offshore current controls extended by the proposed enhancement (red) to allow for onshore contributions.

For an accurate offshore DC voltage estimation, the parameter K_p (see Table 5) is set to 0 in all onshore controls. The parameter K_{vDCon} of the enhancement must equal the onshore DC voltage setpoint v^*_{DC} in per-unit value (1 p.u., see Figure 9) and must be updated by a

one-time communication between the corresponding onshore control and offshore current control, if changed. The value of the parameter K_{DC} can be calculated as

$$K_{DC} = -\frac{v_{rDC}}{2 \cdot R_{HVDC}} \quad (5)$$

using per-unit values. In the grid model, the value is dynamically initialized to avoid transients at the beginning of the simulation and assumed to remain constant. To counteract the transient reduction in the control dynamics introduced by the enhancement, the gain K_{pvd} of the offshore voltage control (see Table 3) is increased from 0.2 to 0.5 p.u. The gain K_{pDC} determines the DC voltage dependency and is set to 7 p.u. This enhancement is implemented in all the offshore current controls in the same way.

6. Feasibility and Effects of Onshore SI and PCR Contributions with the Enhanced Offshore HVDC Converter Controls

In this section, the simulations from Section 4 are repeated to determine the feasibility and effects of contributions using the enhanced offshore controls for the VSC HVDC converters. The initial operating points and grid model variants given in Section 4 still apply.

VSC HVDC connections are considered first, for which the active power schedule is triggered at HVDC 5 in grid model variant 1. As can be seen in Figure 19a, with the enhanced offshore controls, contributions are now feasible for the entire duration of 2.5 s. In analogy to the DRU HVDC connections, the reduced DC voltage (see Figure 20) affects the active power of the corresponding offshore converter, and the active power balance of the offshore grid is met by the remaining VSC HVDC connections (see Figure 19b). Note that all offshore current controls receive updated active current component reference values from the voltage control, but for the response of the offshore converter of HVDC 5, the effect of the local control enhancement is predominant. As a result, during contributions, the active current distribution between the offshore HVDC converters differs from the one defined by the distribution factors in voltage control.

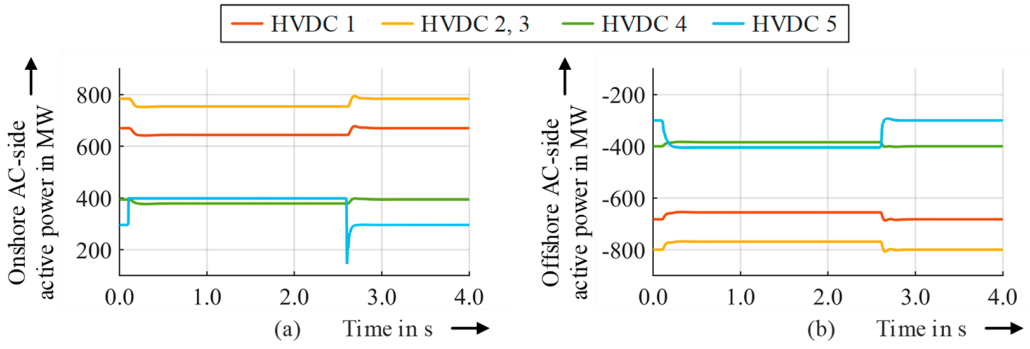

Figure 19. AC-side active power curves of the (**a**) onshore and (**b**) offshore HVDC converters for the active power schedule triggered at HVDC 5 (VSC HVDC connection) in grid model variant 1 using the enhanced offshore controls.

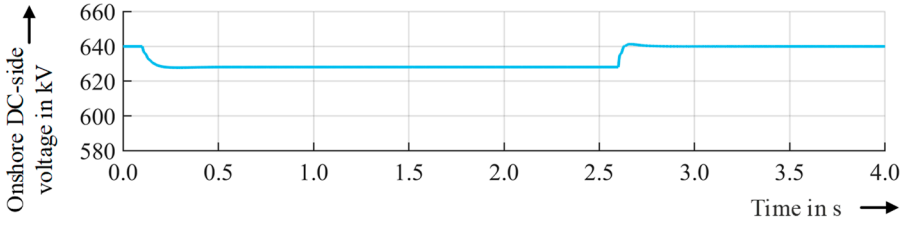

Figure 20. DC-side voltage curve at the onshore converter of HVDC 5 for the active power schedule triggered at HVDC 5 (VSC HVDC connection) in grid model variant 1 using the enhanced offshore controls.

In Figure 20, the DC voltage of 628 kV during the contribution is well above 600 kV, where modulation limits were reached before (see Figure 13). The DC voltage dip during contributions to signal a certain amount of active power to the offshore converter is mainly defined by the value of K_{vDC}. The value reflects a trade-off between a reduced voltage dip (higher value) and better damping in case of rapid active power changes (lower value).

Due to the higher DC voltage at the end of the active power schedule compared to no control enhancement, the transient active power spike caused by the fast DC voltage restoration is significantly less pronounced (see Figures 12a and 19a). While a smoother restoration would be sought in practical contribution implementations, the simplified modeling with fast restoration does not affect the validity of the results of this study.

The active power curves in Figures 21 and 22 show that contributions from VSC HVDC connections are also feasible in other grid model variants. It is worth highlighting that due to the transient impact of the contribution on the offshore AC voltage, the DRU HVDC connections buffer the offshore active power balance until the offshore AC voltage is restored. This negatively affects the contribution dynamics if any DRU HVDC connections lead to the same synchronous area as the contributing VSC HVDC connection.

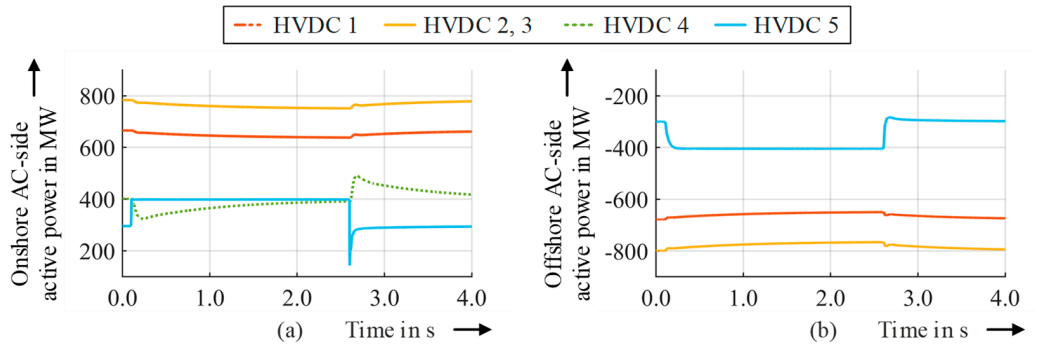

Figure 21. AC-side active power curves of (**a**) all onshore and (**b**) the offshore VSC HVDC converters for the active power schedule triggered at HVDC 5 (VSC HVDC connection) in grid model variant 3 using the enhanced offshore controls.

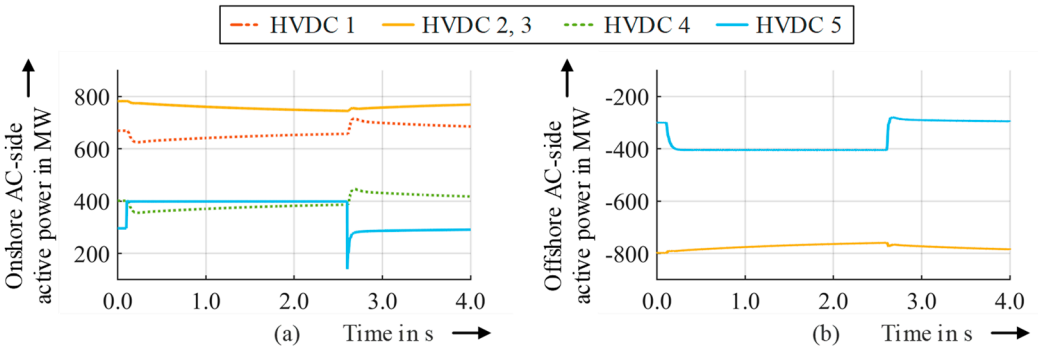

Figure 22. AC-side active power curves of (**a**) all onshore and (**b**) the offshore VSC HVDC converters for the active power schedule triggered at HVDC 5 (VSC HVDC connection) in grid model variant 4 using the enhanced offshore controls.

With regard to the contribution feasibility for DRU HVDC connections, the findings of Section 4 continue to apply when using the enhanced offshore controls. Therefore, the active power and DC voltage curves shown in Figure 23 for the active power schedule triggered at HVDC 4 in grid model variant 4 are almost identical to those in Figure 16. The minor differences are mainly due to the increased proportional gain in the offshore voltage control. An unintended influence of the control enhancement is not observed. For this reason, further plots are omitted.

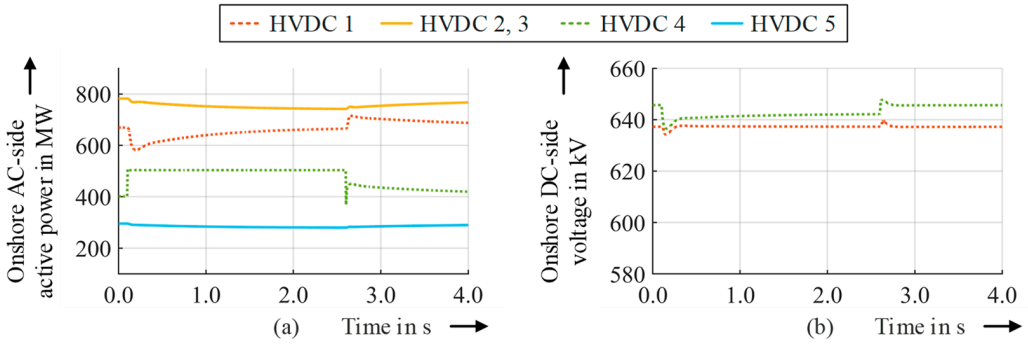

Figure 23. Onshore (**a**) AC-side active power curves of the HVDC connections and (**b**) DC-side voltage curves of the DRU HVDC connections for the active power schedule triggered at HVDC 4 (DRU HVDC connection) in grid model variant 4 using the enhanced offshore controls.

It is to be concluded that the proposed enhancement of the offshore HVDC converter controls grants the feasibility of onshore SI and PCR contributions for both VSC and DRU HVDC connections without the use of communication for the contribution. The required energy is provided by the onshore grid access points of the (non-contributing) VSC HVDC connections by automatically redistributing the active power flow between these HVDC connections.

7. Effects of the Control Enhancement on Normal Operation and Fault Behavior

In the previous section, no unintended influence of the control enhancement on the behavior of the offshore VSC HVDC converter controls was observed. However, as the enhancement is continuously active, this statement cannot be generalized without further simulations. During the development of the applied offshore VSC HVDC converter controls in the German NSON II project, the following deliberately aggravated events were simulated for all four grid model variants to prove the robustness of the controls:

1. Increase in the offshore AC voltage setpoint by 5.7 kV;
2. Decrease in the offshore AC voltage setpoint by 5.7 kV;
3. Increase in the generation of OWP 2 by 360 MW within 200 ms;
4. Decrease in the generation of OWP 2 by 360 MW within 200 ms;
5. Tripping of OWP 4 at the GCP;
6. Three-phase short circuit at node A for 150 ms;
7. Three-phase short circuit in OWP 1 for 150 ms;
8. Tripping of HVDC 2 at the AC side of the offshore converter;
9. Tripping of one cable system between nodes A and C.

The corresponding plots and their explanations can be found in [50]. To determine possible side effects of the control enhancement, all 36 simulations are repeated and the results with and without the enhancement are compared. The comparison shows that the robustness of the offshore HVDC converter controls is still given with the enhancement, as no instantaneous current values harmful to the offshore HVDC converters are observed and a stable operating point is still reached after each event. The slight differences in behavior mainly originate in the increased proportional gain in the voltage control. A small selection of curves is shown in Figures 24–27 to illustrate these findings.

As expected, the increased proportional gain particularly affects the offshore AC voltage curves, e.g., for the voltage setpoint increase in grid model variant 1, depicted in Figure 24a. The similarity of the corresponding active power curves of the offshore VSC HVDC converters with and without the control enhancement (see Figure 24b,c) confirms the active power distribution remaining unaffected by the enhancement. The same finding applies to the OWP generation decrease in grid model variant 4, for which the active power curves of the onshore HVDC converters, given in Figure 25a,b, are indistinguishable.

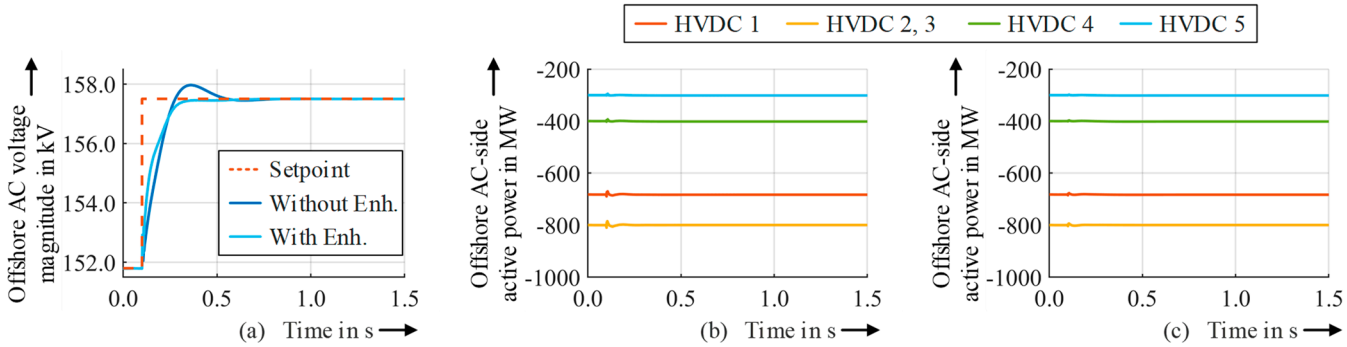

Figure 24. (**a**) Voltage curves at node A; AC-side active power curves of the offshore HVDC converters for the offshore AC voltage setpoint increase (event 1) in grid model variant 1 (**b**) with and (**c**) without the offshore control enhancement.

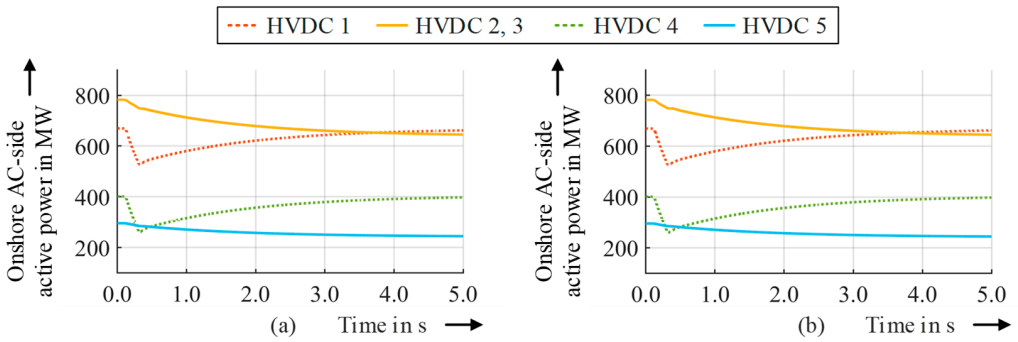

Figure 25. AC-side active power curves of the onshore HVDC converters for the OWP generation decrease (event 4) in grid model variant 4 (**a**) with and (**b**) without the offshore control enhancement.

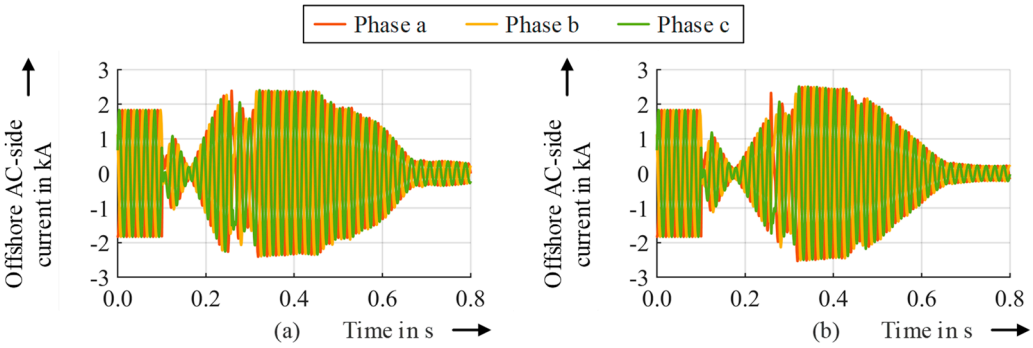

Figure 26. AC-side current curves of the offshore converter of HVDC 2 for the three-phase short circuit at node A (event 6) in grid model variant 3 (**a**) with and (**b**) without the offshore control enhancement.

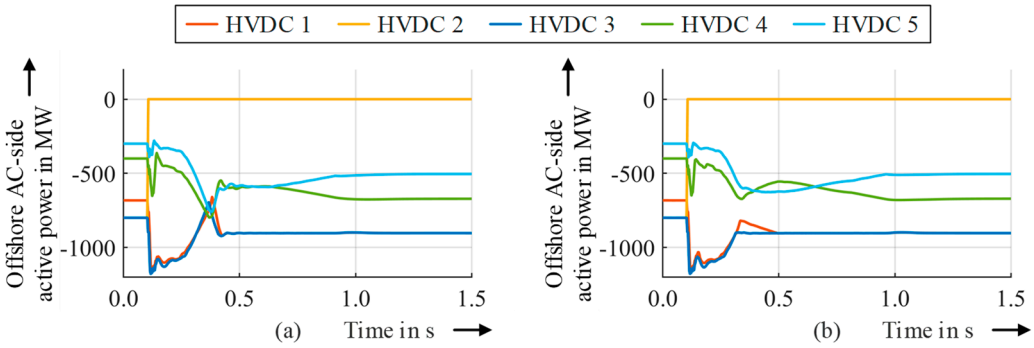

Figure 27. AC-side active power curves of the offshore HVDC converters for the tripping of HVDC 2 (event 8) in grid model variant 1 (**a**) with and (**b**) without the offshore control enhancement.

For the short circuit at node A in grid model variant 3, Figure 26 contains the curves of the phase currents of the most stressed offshore converter (i.e., the one of HVDC 2) until shortly after the fault has been cleared. The return to the initial operating point occurs at roughly 2.5 s. With the control enhancement, a slightly better limitation of the converter currents is observed in the time frame shown; however, this is mainly due to the altered proportional gain in the voltage control. The maximum instantaneous current values reached are 2535 A and 2409 A, respectively. The amplitude of the permitted continuous current of the converter is 2366 A, so no harm to the offshore converters is to be expected.

For the tripping of HVDC 2 in grid model variant 1, the AC-side active power curves of the offshore converters in Figure 27 also show only transient differences with/without using the control enhancement. The functionality of the active power limitation, reached by HVDC 1 and HVDC 3, and the steady-state operating points remain unaffected.

8. Conclusions and Outlook

This article provides a first study on locally triggered onshore synthetic inertia (SI) and primary control reserve (PCR) contributions of an alternating current (AC)-side meshed offshore grid connected by both voltage-source converter (VSC) and diode rectifier unit (DRU) high-voltage direct current (HVDC) connections. As the study focuses on the energetic feasibility and the effects of said contributions on the offshore grid, a simplified onshore contribution modeling is applied.

Simulations show that for onshore contributions of VSC HVDC connections, due to the decoupling of the AC and direct current (DC) voltages commonly used in the offshore converter controls, only the energy stored in the DC link can be accessed, preventing such contributions. For DRU HVDC connections, on the other hand, the inherent dependency of the offshore active power on the DC voltage makes such contributions feasible, as the required energy is automatically taken from the offshore grid, balanced by the VSC HVDC connections collectively acting as a slack, and thus provided by the onshore grid access points of these HVDC connections.

In order to allow locally triggered onshore SI and PCR contributions of both VSC and DRU HVDC connections, a local and continuously active enhancement of the offshore HVDC converter controls based on the inherent DRU converter behavior is proposed. The parameterization of the local enhancement involves system knowledge of the HVDC line resistance and the DC voltage setpoint of the onshore HVDC converter control, the latter requiring updating by one-time communication in case of change. With this minimum system knowledge, the control enhancement allows locally triggered contributions for all onshore HVDC converters without the need for converter preselection. Furthermore, continuous communication is not required and contributions can be made without any communication at all. Although the control enhancement is continuously active and therefore avoids control mode changes, the behavior during normal offshore grid operation is retained and the robustness against various AC-side faults remains. The energy required for contributions is always provided via the onshore grid access points of the non-contributing VSC HVDC connections.

For future work, studies on the active power flow coordination during contributions of SI and PCR are recommended to avoid undermining the purpose of onshore contributions in the case of multiple onshore grid access points being within the same synchronous area. The active power flow coordination is likely to require continuous communication, which also holds for accessing energy retained by the offshore wind parks and their wind turbines, along with modification of their controls. Furthermore, the effects of imprecise system knowledge about the HVDC line resistance and therefore the necessity of more advanced system knowledge integration (e.g., with a thermal model of the resistance) need to be determined to allow for practical implementations. In addition, possible restrictions on the use of the HVDC chopper of VSC HVDC connections introduced by the control enhancement need to be evaluated. This also applies to the use of the HVDC chopper

for DRU HVDC connections in general and includes evaluations of the feasibility of the Emergency Power Control 1 system automatic for both types of HVDC connections.

Author Contributions: Conceptualization, M.H., M.A. and L.H.; methodology, M.H. and M.A.; software, M.H.; validation, M.H. and M.A.; formal analysis, M.H. and M.A.; investigation, M.H. and M.A.; resources, L.H.; data curation, M.H. and M.A.; writing—original draft preparation, M.H.; writing—review and editing, M.H., M.A. and L.H.; visualization, M.H.; supervision, L.H.; project administration, L.H.; funding acquisition, L.H. All authors have read and agreed to the published version of the manuscript.

Funding: This research was supported by the German Federal Ministry for Economic Affairs and Climate Action within the framework of the project "North Seas Offshore Network II: Economical Connection and International Integration of Offshore Wind Energy in the North Sea" (German title: North Seas Offshore Network II: Kosteneffiziente Anbindung und internationale Integration von Offshore Windenergie in der Nordsee, FKZ: 03EI4009). The publication of this article was funded by the Open Access Fund of Leibniz Universität Hannover.

Data Availability Statement: Data are available at https://doi.org/10.25835/0y26b2ml (accessed on 17 July 2023).

Conflicts of Interest: The authors declare no conflict of interest.

References

1. European Parliament. *European Parliament Resolution of 15 January 2020 on the European Green Deal (2019/2956(RSP))*; European Parliament: Strasbourg, France, 2020.
2. European Parliament. *Directive (EU) 2018/2001 of the European Parliament and of the Council of 11 December 2018 on the Promotion of the Use of Energy from Renewable Sources (Recast)*; European Parliament: Strasbourg, France, 2022.
3. Breithaupt, T.; Herwig, D.; Hofmann, L.; Mertens, A.; Meyer, R.; Farrokhseresht, N.; Tuinema, B.; Wang, D.; Rueda Torres, J.; Rüberg, S.; et al. *MIGRATE Deliverable 1.1: Report on Systemic Issues*; MIGRATE Project Consortium: Bayreuth, Germany, 2016. Available online: https://www.h2020-migrate.eu/_Resources/Persistent/9bf78fc978e534f6393afb1f8510db86e56a1177/MIGRATE_D1.1_final_TenneT.pdf (accessed on 17 July 2023).
4. Sewdien, V.N.; van der Meijden, M.; Breithaupt, T.; Hofmann, L.; Herwig, D.; Mertens, A.; Tuinema, B.; Rueda Torres, J.L. Effects of Increasing Power Electronics on System Stability: Results from MIGRATE Questionnaire. In Proceedings of the 2018 International Conference and Utility Exhibition on Green Energy for Sustainable Development (ICUE 2018), Phuket, Thailand, 24–26 October 2018; pp. 1–9.
5. ENTSO-E. *Frequency Stability Evaluation Criteria for the Synchronous Zone of Continental Europe*; ENTSO-E RG-CE SP&D SG: Brussels, Belgium, 2016. Available online: https://eepublicdownloads.entsoe.eu/clean-documents/SOC%20documents/RGCE_SPD_frequency_stability_criteria_v10.pdf (accessed on 17 July 2023).
6. RE-SERVE Project Website. Available online: http://www.re-serve.eu/ (accessed on 17 July 2023).
7. MIGRATE Project Website. Available online: https://www.h2020-migrate.eu/ (accessed on 17 July 2023).
8. European Parliament. *European Parliament Resolution of 16 February 2022 on a European Strategy for Offshore Renewable Energy (2021/2012(INI))*; European Parliament: Strasbourg, France, 2022.
9. Federal Ministry for Economic Affairs and Climate Action. *Ostend Declaration of Energy Ministers on the North Seas as Europe's Green Power Plant*; BMWK: Berlin, Germany, 2023. Available online: https://www.bmwk.de/Redaktion/DE/Downloads/Energie/ostend-declaration-energy-ministers-north-seas-europes-green-power-plant.pdf (accessed on 17 July 2023).
10. ENTSO-E. *ENTSO-E Position on Offshore Development*; ENTSO-E AISBL: Brussels, Belgium, 2020. Available online: https://eepublicdownloads.azureedge.net/clean-documents/Publications/Position%20papers%20and%20reports/2021/entso-e_pp_Offshore_Development_01_200528.pdf (accessed on 17 July 2023).
11. Mende, D.; Harms, Y.; Härtel, P.; Frischmuth, F.; Stock, D.S.; Braun, M.; Herrmann, M.; Hofmann, L.; Valois, M.; Bley, A.; et al. NSON II: Next Steps in Economical Connection and International Integration of Offshore Wind Energy in the North Seas. In Proceedings of the 19th International Workshop on Large-Scale Integration of Wind Power into Power Systems as Well as on Transmission Networks for Offshore Wind Power Plants, Online, 11–12 November 2020; ISBN 9783982008080.
12. Scheufeld, O.; Audichya, Y.; Menze, S.; Wagner, A.; de Groot, N.; Antoine, O.; Henneaux, P.; Karoui, K.; Lessinnes, M.; Mannocchi, A.; et al. *PROMOTioN Deliverable 1.6: Draft Roadmap and Reference Offshore Grid Expansion Plan*; PROMOTioN Project Consortium: Arnhem, The Netherlands, 2017. Available online: https://www.promotion-offshore.net/fileadmin/PDFs/D1.6_Draft_r.oadmap_and_reference_offshore_grid_expansion_plan_-_v1.0.pdf (accessed on 17 July 2023).
13. Nouri, B.; Sørensen, P.; Rudolph, F.; Brantl, C.; Köhler, H.; Adam, G.P.; Li, R.; Bernal-Perez, S. *PROMOTioN Deliverable 2.4: Requirement Recommendations to Adapt and Extend Existing Grid Codes*; PROMOTioN Project Consortium: Arnhem, The Netherlands, 2019. Available online: https://www.promotion-offshore.net/fileadmin/PDFs/D2.4_Requirement_recommendations_to_adapt_.and_extend_existing_grid_codes_final.pdf (accessed on 17 July 2023).

14. Hammer, T.; Slavomir, S.; Menke, P.; Hacker, F.; Szangolies, B.; Meth, J.; Dorn, J.; Loppach, K.; Zurowski, R. *Diode-Rectifier HVDC Link to Onshore Power Systems: Dynamic Performance of Wind Turbine Generators and Reliability of Liquid Immersed HVDC Diode Rectifier Units*; CIGRÉ: Paris, France, 2016.
15. Kuhn, O.; Menke, P.; Zurowski, R.; Christ, T.; Seman, S.; Giering, G.; Hammer, T.; Imamovic, D.; Thisted, J.; Brogn, P.; et al. *2nd Generation DC Grid Access for Offshore Wind Farms: HVDC in an AC Fashion*; CIGRÉ: Paris, France, 2016.
16. Menke, P. 2nd Generation DC Grid Access for Large Scale Offshore Wind Farms. In Proceedings of the Offshore Wind R&D Conference 2015, Bremerhaven, Germany, 13–15 October 2015.
17. PROMOTioN Project Website. Available online: https://www.promotion-offshore.net/ (accessed on 17 July 2023).
18. NSON II Project Website. Available online: https://www.iee.fraunhofer.de/en/research_projects/search/2020/nson-2.html (accessed on 17 July 2023).
19. Henninger, S.; Jaeger, J. Advanced classification of converter control concepts for integration in electrical power systems. *Int. J. Electr. Power Energy Syst.* **2020**, *123*, 106210. [CrossRef]
20. North American Electric Reliability Corporation. *Fast Frequency Response Concepts and Bulk Power System Reliability Needs*; NERC: Atlanta, GA, USA, 2020.
21. Rüberg, S.; Sewdien, V.; Rueda Torres, J.L.; Rakhshani, E.; Wang, D.; Tuinema, B.; Farrokhseresht, N.; Gusain, D.; Perilla, A.; Mola Jimenez, J.; et al. *MIGRATE Deliverable 1.6: Demonstration of Mitigation Measures and Clarification of Unclear Grid Code Requirements*; MIGRATE Project Consortium: Bayreuth, Germany, 2019. Available online: https://www.h2020-migrate.eu/_Resources/Persistent/a7e3d4424f6f749e419ddac011419e7a0aa5f576/D1.6%20-%20Demonstration%20of%20Mitigation%20Measures%20and%20Clarification%20of%20Unclear%20Grid%20Code%20Requirements%20-%20final.pdf (accessed on 17 July 2023).
22. European Commission. *Commission Regulation (EU) 2016/1447 of 26 August 2016 Establishing a Network Code on Requirements for Grid Connection of High Voltage Direct Current Systems and Direct Current-Connected Power Park Modules*; European Commission: Brussels, Belgium, 2016.
23. TenneT TSO GmbH. *Netzanschlussregeln: Hoch- und Höchstspannung*; TenneT TSO GmbH: Bayreuth, Germany, 2022. Available online: https://www.tennet.eu/de/strommarkt/kunden-deutschland/netzkunden/netzanschlussregeln (accessed on 17 July 2023).
24. *Verband der Elektrotechnik, Elektronik, Informationstechnik e. V. VDE-AR-N 4131, Technische Regeln für den Anschluss von HGÜ-Systemen und über HGÜ-Systeme Angeschlossene Erzeugungsanlagen (TAR HGÜ)*; VDE Verlag GmbH: Berlin, Germany, 2019. Available online: https://www.vde-verlag.de/normen/0100511/vde-ar-n-4131-anwendungsregel-2019-03.html (accessed on 17 July 2023).
25. Zhu, J.; Booth, C.D.; Adam, G.P.; Roscoe, A.J.; Bright, C.G. Inertia Emulation Control Strategy for VSC-HVDC Transmission Systems. *IEEE Trans. Power Syst.* **2013**, *28*, 1277–1287. [CrossRef]
26. Zhang, Z.; Lee, J.; Jang, G. Improved Control Strategy of MMC–HVDC to Improve Frequency Support of AC System. *Appl. Sci.* **2020**, *10*, 7282. [CrossRef]
27. Wang, Y.; Zhu, X.; Xu, L.; Li, H. Contribution of VSC-HVDC connected wind farms to grid frequency regulation and power damping. In Proceedings of the 36th Annual Conference of the IEEE Industrial Electronics Society (IECON 2010), Glendale, AZ, USA, 7–10 November 2010; pp. 397–402.
28. Liu, X.; Lindemann, A. Control of VSC-HVDC Connected Offshore Windfarms for Providing Synthetic Inertia. *IEEE J. Emerg. Sel.* **2018**, *6*, 1407–1417. [CrossRef]
29. Pipelzadeh, Y.; Chaudhuri, B.; Green, T.C. Inertial response from remote offshore wind farms connected through VSC-HVDC links: A Communication-less scheme. In Proceedings of the 2012 IEEE Power and Energy Society General Meeting, San Diego, CA, USA, 22–26 July 2012; pp. 1–6.
30. Li, Y.; Zhang, Z.; Yang, Y.; Li, Y.; Chen, H.; Xu, Z. Coordinated control of wind farm and VSC–HVDC system using capacitor energy and kinetic energy to improve inertia level of power systems. *Int. J. Electr. Power Energy Syst.* **2014**, *59*, 79–92. [CrossRef]
31. Junyent-Ferre, A.; Pipelzadeh, Y.; Green, T.C. Blending HVDC-Link Energy Storage and Offshore Wind Turbine Inertia for Fast Frequency Response. *IEEE Trans. Sustain. Energy* **2015**, *6*, 1059–1066. [CrossRef]
32. Wen, L.; Sun, Z.; Hu, H.; Zhang, Y.; Lu, G.; Wu, J.; Dou, Q. A novel frequency support strategy for VSC-HVDC system with large wind power integration. In Proceedings of the 18th International Conference on AC and DC Power Transmission (ACDC 2022), Online Conference, 2–3 July 2022; pp. 666–670.
33. Chu, J.; Lv, Y.; Xu, Y.; Du, G.; Sun, D.; Yu, P. Coordinated Control Strategy for Improving Frequency Stability of Offshore Wind Farms Connected to the Grid through MMC-HVDC Transmission. In Proceedings of the 4th Asia Energy and Electrical Engineering Symposium (AEEES 2022), Chengdu, China, 25–28 March 2022; pp. 354–360.
34. Phulpin, Y. Communication-Free Inertia and Frequency Control for Wind Generators Connected by an HVDC-Link. *IEEE Trans. Power Syst.* **2012**, *27*, 1136–1137. [CrossRef]
35. Lin, C.-H.; Wu, Y.-K. Overview of Frequency-Control Technologies for a VSC-HVDC-Integrated Wind Farm. *IEEE Access* **2021**, *9*, 112893–112921. [CrossRef]
36. Wu, J.; Wang, Z.; Rao, H.; Chen, Y.; Huang, W. A Review of Control Strategies for Inertia Support in VSC-HVDC System. In Proceedings of the 4th IEEE Workshop on the Electronic Grid (eGRID 2019), Xiamen, China, 11–14 November 2019; pp. 1–6.
37. Zhang, H.; Zhu, J.; Guerrero, J.M.; Adam, G.P.; Booth, C.D. A generic inertia emulation controller for multi-terminal VSC-HVDC systems. In Proceedings of the 2nd IET Renewable Power Generation Conference (RPG 2013), Beijing, China, 9–11 September 2013.

38. Bidadfar, A.; Saborío-Romano, O.; Sakamuri, J.N.; Altin, M.; Cutululis, N.A.; Sørensen, P.E. Primary Frequency Support from Offshore Wind Power Plants Connected to HVDC Grids. In Proceedings of the 2019 IEEE Milan PowerTech, Milano, Italy, 23–27 June 2019; pp. 1–6.
39. Tu, L.; Yang, Y.; Yang, J.; Sun, T. The Synthetic Inertia Controller for MMC-HVDC Based Offshore Wind Farm Integration. In Proceedings of the IEEE 1st International Power Electronics and Application Symposium (PEAS 2021), Shanghai, China, 12–15 November 2021; pp. 1–4.
40. Silva, B.; Moreira, C.L.; Seca, L.; Phulpin, Y.; Pecas Lopes, J.A. Provision of Inertial and Primary Frequency Control Services Using Offshore Multiterminal HVDC Networks. *IEEE Trans. Sustain. Energy* **2012**, *3*, 800–808. [CrossRef]
41. Adeuyi, O.D.; Cheah-Mane, M.; Liang, J.; Jenkins, N. Fast Frequency Response From Offshore Multiterminal VSC–HVDC Schemes. *IEEE Trans. Power Deliv.* **2017**, *32*, 2442–2452. [CrossRef]
42. Saborío-Romano, O.; Bidadfar, A.; Sakamuri, J.N.; Göksu, Ö.; Cutululis, N.A. Primary Frequency Response from Offshore Wind Farms Connected to HVdc via Diode Rectifiers. In Proceedings of the 2019 IEEE Milan PowerTech, Milano, Italy, 23–27 June 2019; pp. 1–6.
43. Saborío-Romano, O. *PROMOTioN Deliverable 3.5: Performance of Ancillary Services Provision from WFs Connected to DR-HVDC*; PROMOTioN Project Consortium: Arnhem, The Netherlands, 2018. Available online: https://www.promotion-offshore.net/fileadmin/PDFs/D3.5_PROMOTioN_Performance_of_ancillary_services_pro-vision_from_WFs_connected_to_DR-HVDC.pdf (accessed on 17 July 2023).
44. Xiao, H.; Huang, X.; Huang, Y.; Liu, Y. Self-Synchronizing Control and Frequency Response of Offshore Wind Farms Connected to Diode Rectifier Based HVDC System. *IEEE Trans. Sustain. Energy* **2022**, *13*, 1681–1692. [CrossRef]
45. Xie, L.; Yao, L.; Li, Y.; Xu, L.; Wang, Z.; Wei, C.; Fan, C. Frequency regulation participation of offshore wind farm integrated by diode-rectifer HVDC system. *J. Eng.* **2019**, *2019*, 977–981. [CrossRef]
46. Saborío-Romano, O.; Bidadfar, A.; Sakamuri, J.N.; Zeni, L.; Göksu, Ö.; Cutululis, N.A. Communication-Less Frequency Support From Offshore Wind Farms Connected to HVdc via Diode Rectifiers. *IEEE Trans. Sustain. Energy* **2021**, *12*, 441–450. [CrossRef]
47. Saborío-Romano, O.; Bidadfar, A.; Sakamuri, J.N.; Göksu, Ö.; Cutululis, N.A. Fast Frequency Response from Offshore Wind Farms Connected to HVDC via Diode Rectifiers. In Proceedings of the 2019 CIGRÉ Aalborg International Symposium, Aalborg, Denmark, 4–7 June 2019.
48. Herrmann, M. *Dataset: PowerFactory EMT Model of a Meshed AC Offshore Wind Park Grid Connected by Five HVDC Connections*; Leibniz University Hannover: Hanover, Germany, 2023. [CrossRef]
49. Herrmann, M.; Hofmann, L. *AP 2: Anlagen- und Systemregelung AS 2.2: Entwicklung von Regelungskonzepten zum Parallelbetrieb von HGÜ-Umrichterstationen*; NSON II Project Consortium: Kassel, Germany, 2021. Available online: https://publica.fraunhofer.de/entities/publication/e0ed1845-19c8-41e1-bdde-08608591c684/details (accessed on 17 July 2023).
50. Herrmann, M.; Hofmann, L. *AP 2: Anlagen- und Systemregelung AS 2.3: Entwicklung von Regelungskonzepten zum Betrieb von HGÜ-Umrichterstationen in Drehstromseitig Vermaschten Offshore-Netzen*; NSON II Project Consortium: Kassel, Germany, 2022. Available online: https://publica.fraunhofer.de/entities/publication/611c3204-57df-467c-80f0-90b36b1f006b/details (accessed on 17 July 2023).
51. Korai, A.W. Dynamic Performance of Electrical Power Systems with High Penetration of Power Electronic Converters: Analysis and New Control Methods for Mitigation of Instability Threats and Restoration. Doctoral Thesis, Universität Duisburg-Essen, Duisburg, Essen, Germany, 2019.
52. TenneT TSO GmbH. *Offshore-Netzanschlussregeln*; TenneT TSO GmbH: Bayreuth, Germany, 2019.
53. Weber, H.; Baskar, P.; Ahmed, N. Power system control with renewable sources, storages and power electronic converters. In Proceedings of the 2018 IEEE International Conference on Industrial Technology (ICIT 2018), Lyon, France, 20–22 February 2018; pp. 1272–1278.
54. Herrmann, M.; Hofmann, L. Enhancement of a Control Concept for Parallel HVDC Link Operation to Increase Flexibility for Offshore Wind Park Grid Connections. In Proceedings of the 12th International Renewable Energy Congress (IREC 2021), Hammamet, Tunisia, 26–28 October 2021; pp. 1–8.
55. Lopez, M.; Briz, F.; Zapico, A.; Diaz-Reigosa, D.; Guerrero, J.M. Operation of modular multilevel converters under voltage constraints. In Proceedings of the 2015 IEEE Energy Conversion Congress and Exposition (ECCE 2015), Montreal, QC, Canada, 20–24 September 2015; pp. 3550–3556.
56. Qoria, T.; Cossart, Q.; Li, C.; Guillaud, X.; Colas, F.; Gruson, F.; Kestelyn, X. *MIGRATE Deliverable 3.2: Local Control and Simulation Tools for Large Transmission Systems*; MIGRATE Project Consortium: Bayreuth, Germany, 2018. Available online: https://www.h2020-migrate.eu/_Resources/Persistent/5c5beff0d5bef78799253aae9b19f50a9cb6eb9f/D3.2%20-%20Local%20control%20and%20simulation%20tools%20for%20large%20transmission%20systems.pdf (accessed on 17 July 2023).
57. DIgSILENT GmbH. *Technical Reference Documentation Phase Measurement Device: ElmPhi_pll*; DIgSILENT GmbH: Gomaringen, Germany, 2019.